Exp. Theo. NANOTECHNOLOGY 3 (2019) 247-261

Experimental and Theoretical
NANOTECHNOLOGY
http://etn.siats.co.uk/

Si-doped polycrystalline via chemical deposition

D.B. Devedov[1-*], R.J. Asherov[1], G.H. Glenko[1], N.O. Ferstaloya[2]

[1]*General Physics Institute RAS, Vavilov str. 38, Moscow 119991, Russia*
[2]*BelarusianStateUniversity, Nezavisimosti av. 4, Minsk, 220030, Republic of Belarus*
**) E-mail: devedov@yandex.ru*

Received: 2/2/2018 / *Accepted:* 24/7/2018 / *Published:* 1/9/2019

Abstract: Microcrystalline diamond films doped with silicon have been grown on aluminum nitride substrates by a microwave plasma CVD. The doping has been performed via adding silane in various concentrations to CH4–H2 reaction gas mixture in course of the deposition process. The films produced at the substrate temperatures of 750 to 950°C have been characterized by SEM, AFM, Raman and photoluminescence (PL) spectroscopy to assess the effect of Si doping on the diamond structure. The doped films showed bright photoluminescence of silicon-vacancy (SiV) color centers at 738 nm wavelength as well as noticeable side band at 723 nm. The optimum doping condition (SiH4/CH4 = 0.6%), that maximize the SiV PL emission, was determined for the range of silane concentrations SiH4/CH4 (0.0 – 0.9%) explored. A further PL enhancement can be achieved by increase in the substrate temperature. The applied *in situ* doping from gas phase is shown to be an easy and effective method to incorporate Si in diamond in a controllable way.

Keywords: CVD; AlN; PL.

1. INTRODUCTION

Chemical vapor deposition (CVD) diamond films are of high research and industrial interests due to extreme hardness and thermal conductivity, low wear, wide transparency window, biocompatibility, and a bouquet of other unique properties, making this material important in tool manufacturing, IR and RF optics, biomedicine [1-5]. The doping of the films with nitrogen and silicon to form bright color centers, such as nitrogen vacancy (NV) or silicon-vacancy (SiV) in diamond is demanded for applications in quantum information technologies [6, 7] and optical biomarkers [8, 9]. Also, The Si-doped diamond films display excellent

tribological properties due to reduced friction Coefficient compared to undoped or B-doped films [10]. Thus, the doping of diamond coatings with Si looks promising both for photonic and mechanical applications. However, only limited number of works can be found in the literature on *in situ* CVD diamond doping with silicon from gaseous precursors in course of the films deposition [11-13], this being in contrast to the doping with other elements like N, P or B, for which the *in situ* doping is well established approach. Musale *et al*. [11] used SiH_4 to dope polycrystalline films grown by hot-filament CVD in CH_4/H_2 mixtures. Grudinkin *et al*. [12] deposited the Si-doped luminescent micrometer-sized isolated particles in microwave (MW) plasma with SiH_4 as a dopant source. In both works it was found that the films grown at high enough silane concentrations has a more defective microstructure and contains a significant amount of amorphous carbon phase. As the alternative to silane the tetraethoxysilane ($C_8H_{20}O_4Si$) was used to deposit diamond films on silicon substrates [13], and WC-Co substrates [10] in hot-filament CVD systems. The emission of SiV defects at 738 nm wavelength in photoluminescence spectrum was the only indicator of the successful Si doping in those films. Recently [14] we briefly reported on PL characterization of thin films on aluminum nitride substrates deposited by MPCVD by adding SiH_4 in process gas. Here we present new results on microcrystalline diamond coatings produced in various regimes on the AlN substrates using monosilane gas for the doping.

2. EXPERIMENTAL

The diamond films were deposited on 10x10x0.5 mm^3 polished AlN substrates in the microwave plasma CVD system ARDIS-100 (2.45 GHz) [21] in CH_4/H_2 gas mixtures, adding SiH_4 in variable concentration, under the following process parameters: total gas flow 500 sccm, gas pressure of 70 - 85 Torr and microwave power 2.5 – 3.8 kW. Two series of the films were produced. In one experiment the silane vs methane gas flow ratio (SiH_4/CH_4) was varied from 0% (no silane addition) to 0.9%, while the microwave power (3.3 kW), gas pressure (75 Torr) and substrate temperature 800 ^oC was kept constant. Another batch of the samples was prepared at the substrate temperature varied from 750^oC to 950^oC, as measured by a two-color pyrometer (Willamson 81-35-C) by successive increase of microwave power at pressure 80 Torr, keeping constant the SiH_4/CH_4 ratio of 0.6%. Prior the deposition, the

substrates were seeded in a water-based slurry of detonation nanodiamond (particle average size ~5 nm, 0.2wt%) by ultrasonic treatment for 15 minutes to achieve high diamond nucleation density of 10^9–10^{10} cm^{-2}. The AlN substrates were intentionally chosen instead of conventional Si substrates in order to avoid any interfering Si self-doping from the substrate material via the substrate etching by atomic hydrogen of the plasma.

For correct comparison of the films obtained at different process parameters, their thickness was kept always the same (1000±50 nm). The film thickness and growth rate were measured *in-situ* with a laser interferometry technique [15] (Figure **1**). The growing film was illuminated by a semiconductor laser (A_{las}=656 nm wavelength) through a quartz window on top of the CVD reactor. The laser reflectivity oscillations in time $R(t)$, caused by interference in the film/substrate structure, were monitored by a portable spectrometer (Ocean Optics 4000). The distance between two neighbor maxima in the $R(t)$ signal corresponds to $A_{las}/2n$ 136 nm increment in the film thickness, where n=2.4 is the refraction index of diamond. No band-pass optical filter was needed to cut off the background radiation from the plasma due to high signal-to-noise ratio within narrow spectral interval around the laser wavelength.

The film surface morphology and grain size were examined with scanning electron microscopy (SEM) using Tescan MIRA3 and FEI Quanta 600 instruments. Raman spectroscopy and photoluminescence spectra were taken at room temperature (R.T.) with LABRAM HR-800 spectrometer equipped with a diode-pumped solid-state laser (A = 473 nm). The laser beam was focused in =1 μm spot on the sample surface. The spectra were taken in three different locations within the central zone of each sample to assess uniformity of the samples. The variations in the intensity, peak position and width of the 1^{st} order Raman peals and PL SiV line were typically less than 10%. The averaged parameters of the Raman and PL lines were used to analyze the trends in the spectra with the doping.

In addition, the mapping of intensity PL line at 738 nm wavelength was performed at R.T. with the Integra Spectra system (NT-MDT) using the spectra excitation with a He-Ne laser at 632 nm. The laser beam was focused in a spot of = 0.8 μm diameter and scanned across an area of up to 30x30 μm^2 (200x200 pixels) to produce the SiV PL intensity surface distribution. The apparatus allowed measurement of the surface relief by atomic force microscopy at the same area where the PL map is taken.

3. RESULTS AND DISCUSSION

3.1. SEM Characterization

In general, the undoped film and the films doped with Si at different silane addition in gas at fixed deposition temperature Td=800^{O}C exhibited similar morphologies, but different grain sizes. The SEM images of undoped and most heavily doped (SiH_4/CH_4 = 0.9%) samples are shown in Figure **2**. Both films consist of randomly oriented well faceted crystallites, with dimensions of 300-500 nm for the undoped film, enlarged to 500-800 nm for the doped ones.

The film structure was sensitive to the deposition temperature Td. The SEM images of the growth surfaces for five films produced at different Td at fixed silane content in gas mixture (SiH_4/CH_4 = 0.6%) is shown in Figure **3**. While the surface morphology remains unchanged at low temperatures of 750- 850^{O}C, a tendency for grain size decrease and more twin's appearance is observed for higher Td.

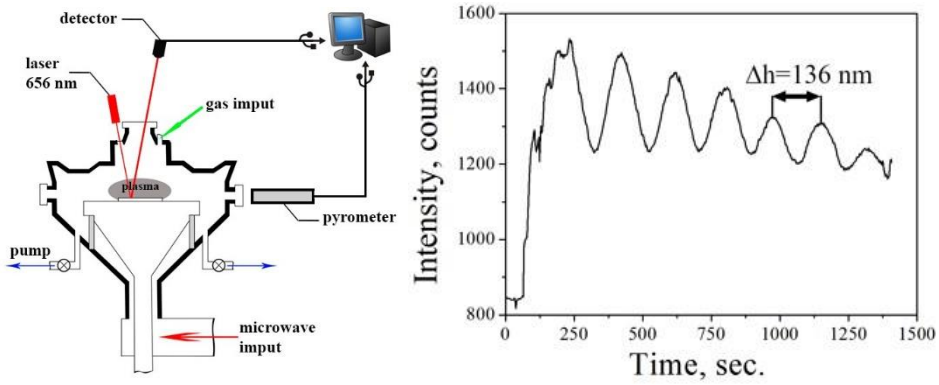

Figure 1: Schematics of *in situ* measurement of the film thickness by laser interferometry upon the diamond deposition (left) and typical reflection vs time oscillations (right).

Exp. Theo. NANOTECHNOLOGY 3 (2019) 247-261

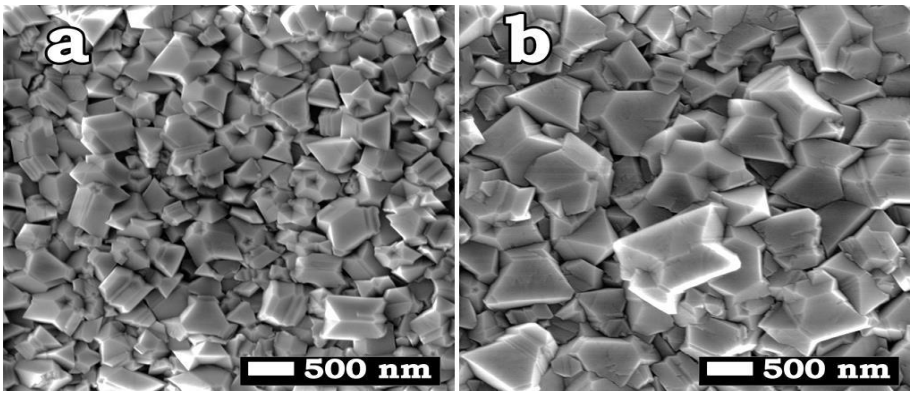

Figure 2: SEM images of undoped (**a**) and Si-doped at SiH_4/CH_4 = 0.9% (**b**) microcrystalline diamond films deposited at T_d=800^{o}C.

3.2 Growth Rate

An almost constant growth rate of 1.5±0.15 μm/h was determined for the films produced at T_d=800^{o}C at different

SiH_4/CH_4 ratios as shown in Figure **4a**. In contrast, the growth rate increases almost linear from 0.7 to 2.6 μm/h with T_d elevation for the films deposited at SiH_4/CH_4 = 0.6% (Figure **4b**). Note, that at the substrate temperature 800^{o}C the growth rate for the sample from of the second batch (Figure **4b**) is somewhat lower (1.25 μm/h) compared to that for the films with variable Si doping (Figure **4a**). This difference in growth rates comes from the slight difference in deposition conditions of the particular samples, the former being produced at microwave power of 3.3 kW and pressure of 75 Torr, while the latter at the microwave power of 3.0 kW and pressure of 80 Torr. Important, that the crystallinity of the films does not degrade with the growth rate as deduced from corresponding Raman spectra.

3.3 Raman Spectra

The Raman spectra for the films obtained at T_d=800^{o}C at different doping levels are shown in Figure **5**. The spectra reveal the following features common for polycrystalline diamond films: (i) then arrow diamond peak at =1336 cm^{-1}, (ii) two wide bands from trans-polyacetylene (t-PA) at 1140 cm^{-1} and 1480 cm^{-1}, and (iii) D- and G-peaks at 1350 cm^{-1} and 1580 cm^{-1}, respectively, from graphitic carbon [16]. The sp^2/sp^3 ratio, expressed as the

Exp. Theo. NANOTECHNOLOGY 3 (2019) 247-261

ratio of the sum of D- and G- peaks integrated intensities (areas under the bands) to that for 1336 cm^{-1} peak, is shown in Figure **6** in dependence of silane percentage added. For this analysis the diamond line at 1336 cm^{-1} was approximated by a Lorentzian profile, and the G- and D-peaks by two Gaussians. No increase in sp^2 contribution to the entire spectrum is revealed for in the explored SiH4/CH4 concentration range.

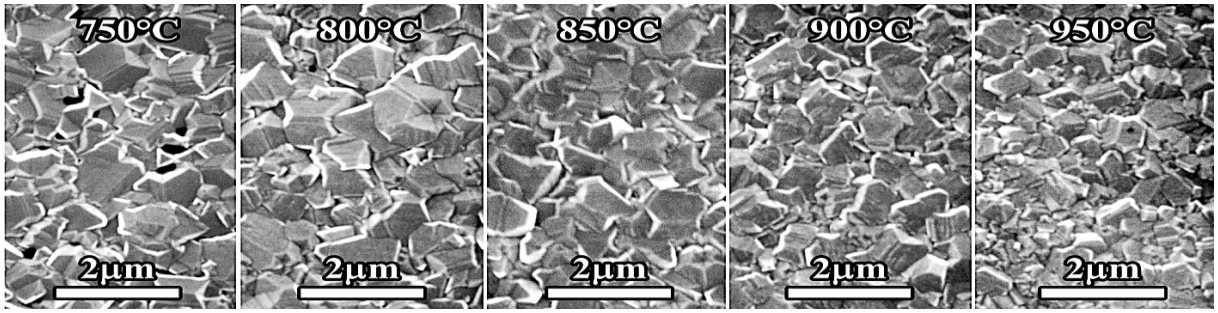

Figure 3: SEM images of Si-doped at SiH4/CH4 = 0.6% diamond films grown at different substrate temperatures.

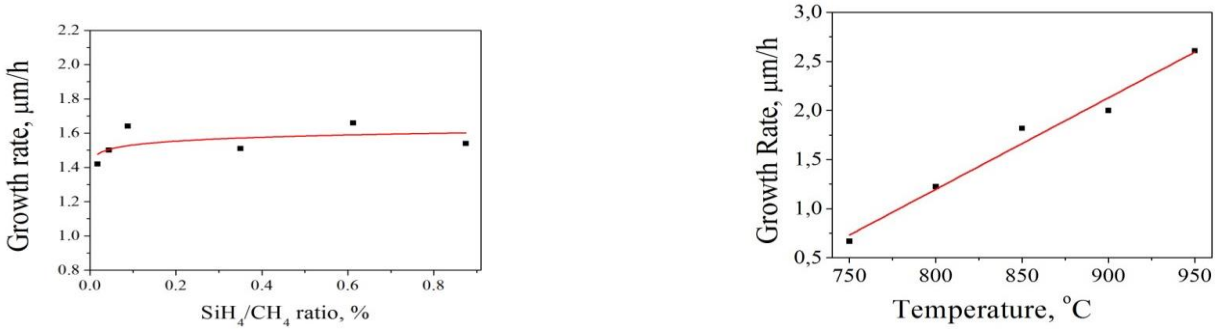

(**b**)

Figure 4: Dependencies of growth rate for the diamond films on SiH4/CH4 ratio at substrate temperature Td=800°C (**a**), and on substrate temperature at SiH4/CH4 = 0.6% (**b**).

Exp. Theo. NANOTECHNOLOGY 3 (2019) 247-261

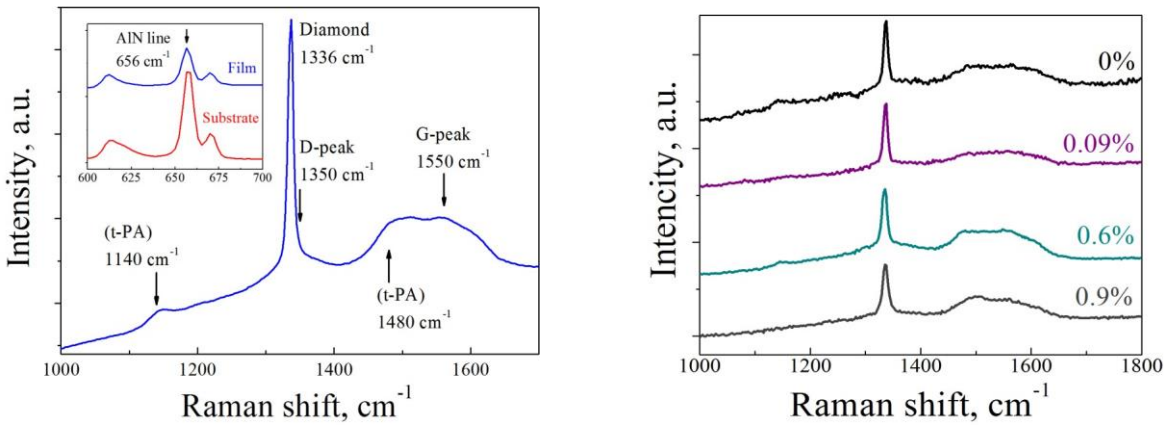

Figue 5: Raman spectra for the films grown at Td=800^{o}C at different SiH4/CH4 ratios in gas. Inset: Raman spectra in low frequency range for the bare AlN substrate and for the film produced at SiH4/CH4= 0.9%, showing AlN spectrum.

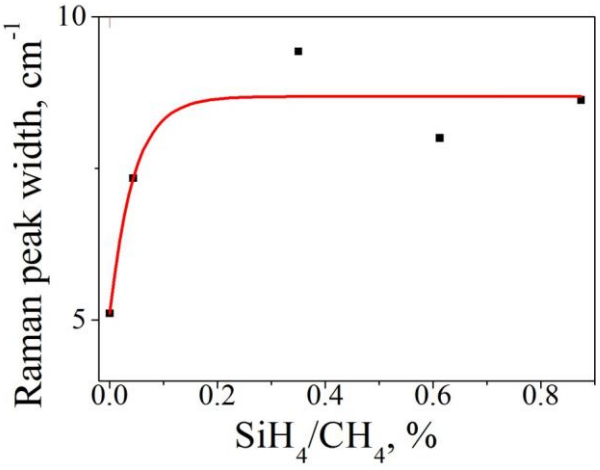

Figure 6: Diamond Raman peak width versus SiH4/CH4 ratio in gas at Td=800ºC.

At small addition of the silane a slight broadening of diamond Raman peak is observed, the full width on half magnitude (FWHM) increasing from 5.0 cm^{-1} for undoped film to 7.5 cm^{-1} for 0.04% SiH4 sample. This might be caused by Si incorporation and a nonuniform stress developed as a consequence of the doping. However, no systematic further broadening of 1336 cm^{-1} peak and no obvious degradation of the film structure at stronger doping can be deduced from the Raman analysis. The diamond films are found to be under compressive

stress of thermal origin due to difference in thermal expansion coefficient (TEC) of AlN (mean value of a = 4.5 x10^{-6} K^{-1} for the 20-500°C range [17]) and diamond (1.0 x10^{-6} K^{-1}). The expected bi-axial thermal stress due to this mismatch is cr = Ella (Td – T0)/(1-μ) = 3.1 GPa, where E = 1040 GPa is Young's modulus, μ = 0.07 is Poisson's ratio, lla is difference in TEC for AlN and diamond, and Td is deposition temperature. The expected stress-induced diamond Raman peak shift llv is then calculated as llv[cm^{-1}]= 2.05cr[GPa] [18] to give llv= 6.3cm^{-1}, leading to the peak position of 1338.8 cm^{-1}, while we measured the Raman peak position at 1336.1±0.2 cm^{-1} (cr = 1.8 GPa), somewhat less than the estimate based solely on thermal stress. A partial stress relaxation and/or a tensile intrinsic stress in the films could result in this difference.

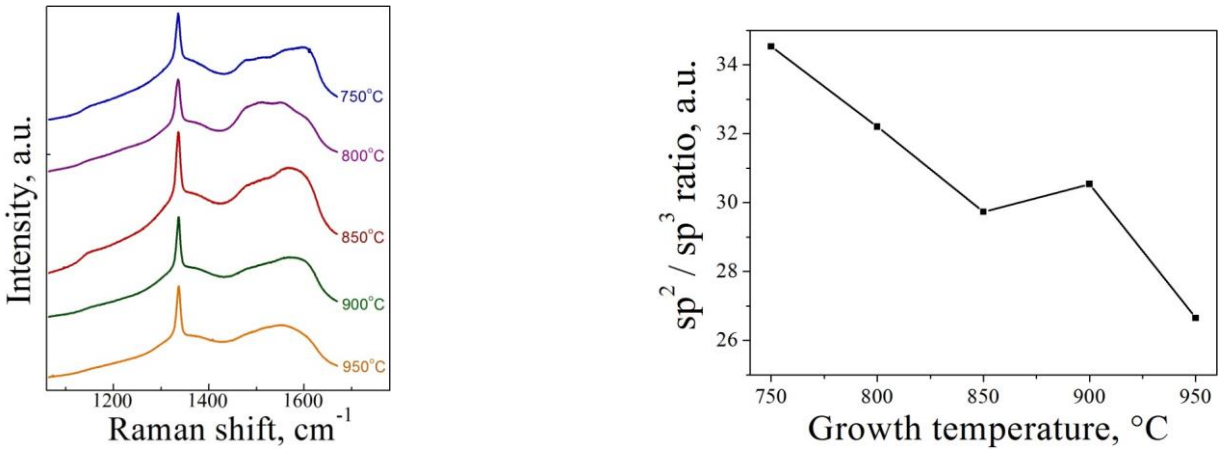

Figure 7: Raman spectra (left) and sp^2/sp^3 ratio for films prepared at different substrate temperatures at SiH4/CH4 = 0.6% (right).

The diamond peak near 1336 cm^{-1}, and the features assigned to amorphous carbon and t-PA, similar to those seen in Figure

5. The sp^2/sp^3 ratio reduces by ~30% with the substrate temperature increase from 750 to 950°C (Figure **7**), indicating some improvement in diamond phase purity. The diamond Raman peak position was tending to increase from 1336.5 cm^{-1} (750^{o}C) to 1338.1 cm^{-1} (950^{o}C), corresponding to increase in compressive stress for the films. FWHM of the

diamond peak, on the other hand, decreased from 7.4 (750^{O}C) nm to 5.8 nm (950^{O}C).

3.4 Photoluminescence Spectra

The PL spectra for the set of the films grown at different SiH4 percentage added in gas are shown in Figure **8**. The PL spectra for all samples exhibit a strong SiV peak at 738 nm, with intensity much higher than that of Raman peak. No nitrogen-related PL peaks, NV^0 (575 nm) or NV^- (637 nm), are observed, indicating negligible, if any, etching of AlN substrate by plasma. The nominally undoped film (no silane added) yet shows a weak SiV peak as a result of silicon contamination in the film due to unintentional plasma etching of Si-containing layers on the reactor chamber walls accumulated from previous doping experiments.

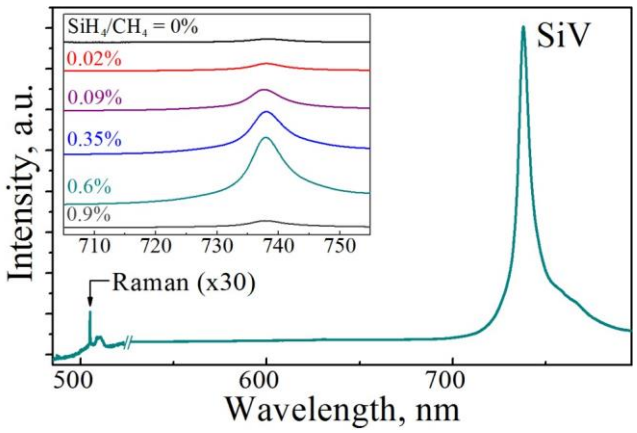

Figure 8: PL of diamond films grown at different SiH4/CH4 ratios, demonstrating the strong peak at 738 nm belonging to SiV defect. Note a decrease in PL for most doped sample (SiH4/CH4 = 0.9%).

The most interesting observation is a nonmonotonic evolution of the SiV peak intensity with the SiH4/CH4 ratio in gas: first, the PL at 738 nm increases at low 0%–0.6% SiH4/CH4 concentrations, then it drops at further SiH4 addition. The plot for integrated SiV PL signal (the area under peak), normalized to integrated diamond Raman peak intensity, against silane content in gas, is displayed in Figure **9**. The SiV PL width (FWHM) tivSiV of 7.3±0.5 nm showed no trend with SiH4 addition. Also, the SiV PL line position for all samples was in the narrow range of 738.3±0.3 nm, being shifted by 0.2 nm to shorter wavelengths in comparison

with the ZPL position of 738.5±0.3 nm in low-strained homoepitaxial diamond films [19]. This 0.2 nm shift can be ascribed to the compressive stress in our films as deduced from Raman analysis. We were not able to find in literature the data on the SiV PL shift with the biaxial applied stress. Sternschulte *et al*. [20] measured the SiV ZPL position under uniaxial stress a for homoepitaxial diamond film along the <001> crystal direction at low (10K) temperature. They observed a splitting of ZPL for a doublet, and the linear shift of the main component of the doublet (1682 meV) with the stress with the rate of –2 meV/GPa (or +0.8 nm/GPa), while the second component revealed a shift to positive energies. The integrated shift of ZPL is by order of magnitude lower (~0.2 nm/GPa), as a result of this compensation. In our case f the expected ZPL shift is ~0.35 nm or the measured stress.

Figure 9: Dependence of integrated SiV PL intensity on SiH4/CH4 ratio used to deposit diamond films at 800°C. The integrated SiV intensity is normalized to integrated diamond Raman peak intensity at 1336 cm^{-1}. The solid line is the guide for eyes.

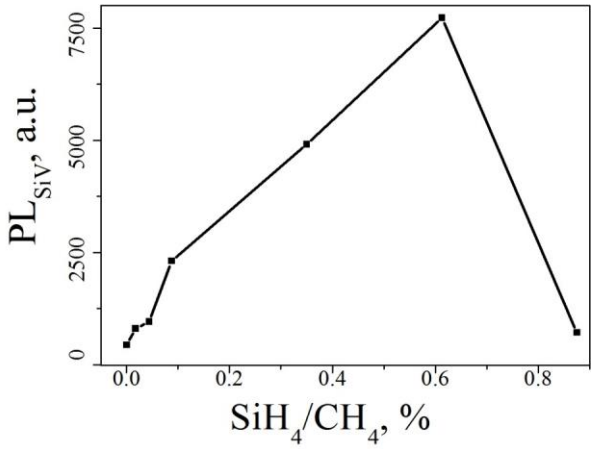

The existence of an optimum silane concentration in gas to maximize the SiV PL intensity has been observed by other authors [11-13]. The PL quenching in isolated microscale diamond particles grown by microwave plasma CVD was explained [12] by increase of amorphous carbon (a-C) impurity abundance in diamond at high silane contents (>0.08%), as confirmed by Raman spectra. The SiV PL decrease in MCD films deposited on Si substrates by a hot filament CVD at silane concentrations above 0.4% has been attributed [11] to the effect of concentration quenching of the luminescence via nonradiative energy dissipation. In contrast, we did not reveal, on the basis of the Raman spectra, a significant degradation of the film

structure in terms of sp^2/sp^3 ratio or diamond Raman peak width (Figure **5**) even at highest SiH4/CH4 concentrations. Therefore, we don't ascribe the PL quenching to Si-induced a-C formation in the films, while some defects caused by Si incorporation in diamond may play a role, those defects, however, not manifesting itself in the diamond Raman peak broadening. The measurements of total Si concentration by secondary ion mass spectrometry (SIMS) in the 0.6% SiH4/CH4 sample (with the brightest PL) and the 0.9% SiH4/CH4 sample (with quenched PL), determined high values of ca. 4000 ppm and 9000 ppm for these films, respectively [21]. Recently [19] we observed a similar effect of PL SiV quenching in epitaxial diamond films also doped from silane, and we found a significant broadening of PL SiV line width at low temperatures (T=5 K) for the single crystal samples with quenching PL, while no change in diamond Raman peak and the 738 nm ZPL width has been seen at R.T. It was concluded [19] that the ZPL width is much more sensitive to defects in the direct vicinity of the SiV centers than the Raman line is. Qualitatively we explained this difference in sensitivity in the following way. The large Si atom disturbs the diamond lattice around its position inducing a local strain field. The formation of SiV center could also be accompanied by appearance of strain and point defects is its vicinity. The total volume of the strained (defective) domains is relatively small, and it contributes a little to Raman spectrum, but the SiV ZPL is more sensitive, it can be broadening at low temperatures due to proximity of the SiV center to those defects. The ZPL broadening was possible to see owing to initially small width (ti}737 = 0.3 nm) of ZPL at T=5 K for low-doped (less than 0.6% SiH4/CH4) homoepitaxial samples, while no increase in ZPL width at room temperature with Si doping was observed because of the ZPL large width (~ 7 nm) at R.T. Similar consideration can be applied for polycrystalline diamond films as well. The local stress could be caused by a variety of defects such as interstitial atoms, Si impurity atoms or their aggregations, and other structural point or extended defects. What particular defect triggers the PL quenching remains, however, unclear at present time.

The mapping of the PL SiV emission over 30x30 μm was performed for one the doped film, and compared with the AFM image of the relief, taken by the same instrument (Figure **10**). The chosen field of view included a large number (~100) of the grains to get enough statistics for 738 nm line intensity distribution. The PL map shows a grainy pattern (Figure **10b**), the

brightest area not necessarily coincide with relief's protrusions. The spotty PL distribution might be a result of anisotropy in Si incorporation probability in different facets of the crystallites (the phenomenon well known, for example, for nitrogen incorporation in HPHT diamond) [22]. Another reason can be connected to angle diagram of the SiV emission. The SiV defects are aligned along <111> directions [23], the SiV dipoles emit perpendicularly to <111>, therefore the (111) planes, when oriented perpendicularly to

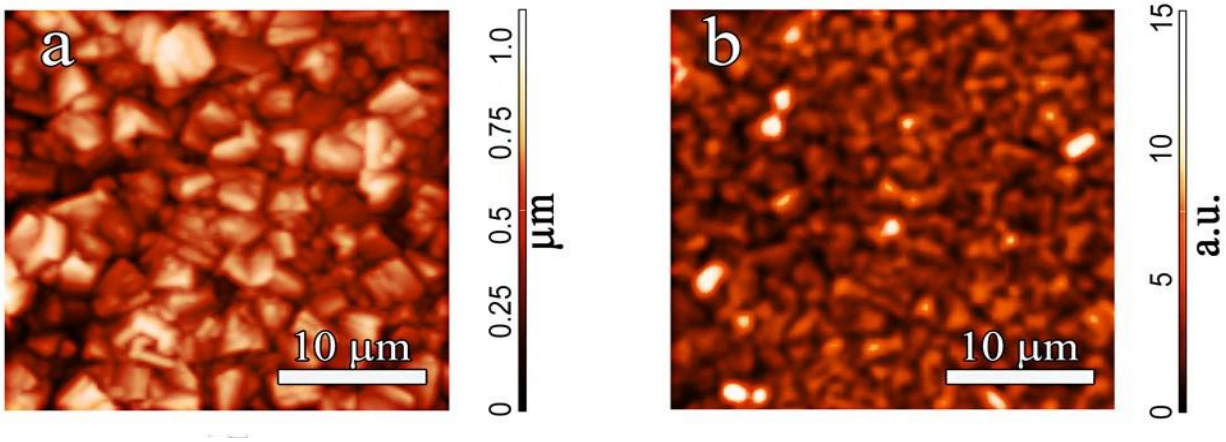

Figure 10: AFM image of a Si-doped microcrystalline diamond film grown at SiH4/CH4 = 0.6% (**a**), and 738 nm PL map for the same region (**b**). The PL excitation was at 632 nm.

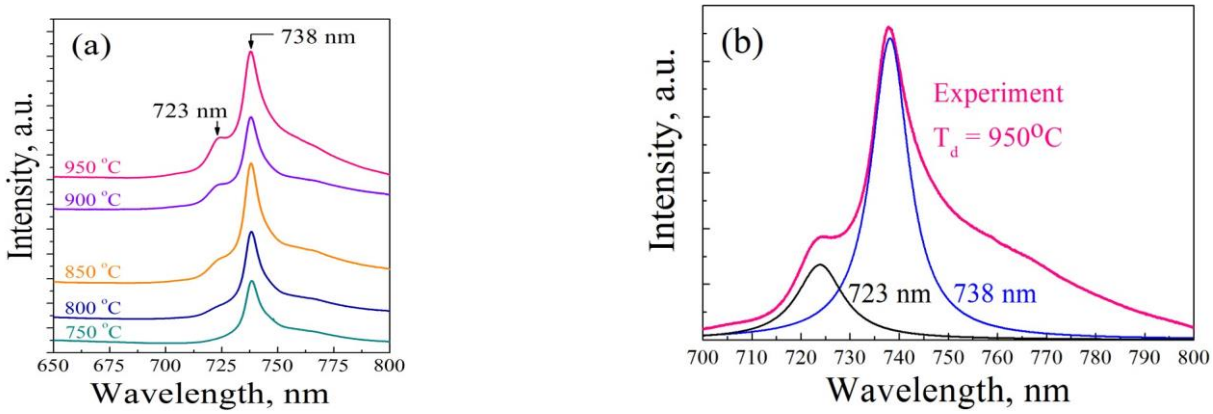

Figure 11: PL spectra for the films grown at different substrate temperatures at SiH4/CH4 = 0.6% (**a**) and approximation of experimental line with two Lorentzians (**b**). Note the appearance of a side band at 723 nm for T_d>800^{o}C.

the excitation beam, make largest contribution to emission collected with the objective of optical microscope viewing normally to the sample surface. In addition, the grains of better quality could promote the stronger PL yield. The SiV PL intensity demonstrates a monotonic

increase with the substrate temperature beginning with = 750^{O}C (Figures **11** and **12**), the ZPL at 738 nm rising approximately twice at Td = 950^{O}C. This indicates that the choice of the optimal substrate temperature can maximize the 738 nm line emission. In addition, a side band at 723 nm appears and enhances together with SiV peak intensity at Td> 800^{O}C (Figures **11** and **12**). This band is not the vibronic one as it lies in anti-Stokes range. Turukhin *et al*. [24] observed the 723 nm peak for free-standing polycrystalline diamond films grown on Si substrate and ascribed it to sp^2 nondiamond carbon phase. Similar peak has been reported by Davydov *et al*. [25] for Si-doped micro-and nanocrystalline diamond particles synthesized by HPHT technique who also treated it as a PL signal from a graphite-like contamination. In our case, however, the intensity of the 723 nm band is much stronger relative to ZPL at 738 nm (the integrated 723 nm band it amounts up to 50% of that for ZPL (Figure **12**) than in those works, and the band width of 15-30 nm seems to be too small compared to typical PL bands related to a-C phase [26, 27]. Moreover, the contribution of non-diamond carbon in the Raman spectra reduces with Td as seen in Figure **7**. This brings into a question the assignment of 723 nm band to a graphitic carbon, so the origin of the 723 nm band, to our opinion, is needed in a further study.

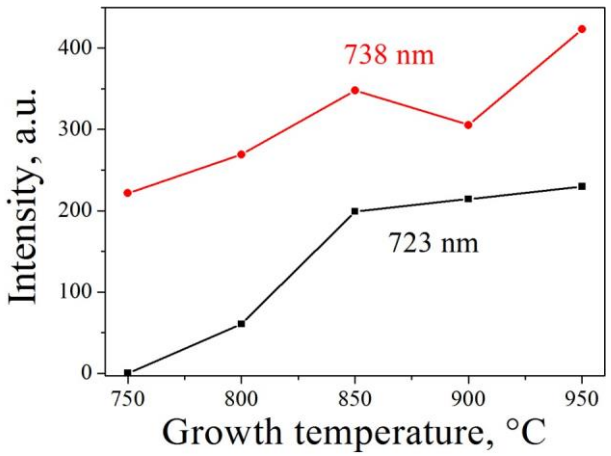

Figure 12: Dependence of integrated intensities for ZPL at 738 nm and the 723 nm side-band in PL spectra for the films grown at different substrate temperatures at SiH4/CH4 = 0.6%.

4. CONCLUSIONS

We produced microcrystalline diamond films on AlN substrates with bright PL of SiV color centers at 738 nm wavelength using a microwave plasma CVD technique. The PL intensity is controlled by doping the films with Si via adding silane to CH_4–H_2 gas mixtures in the course of the deposition process. Within the SiH_4/CH_4 ratios explored (0 – 0.9%) the dependence of SiV PL intensity of the films on the silane concentration in gas shows a maximum at certain SiH_4/CH_4 ratio followed by the PL quenching at high doping levels. No relation of this quenching effect with amorphous carbon formation is established. The applied *in situ* doping from gas phase is an easy and effective way to incorporate Si in diamond. The Si-doped microcrystalline films can be a convenient starting material for preparation of luminescent CVD diamond nanoparticles [8]. In addition, by doping from silane, localized PL SIV emitters can be grown using selective area seeding [28] or direct growth of diamond film through windows in a mask on diamond substrate [29], as it was demonstrated previously with solid Si dopant sources.

References

[1] H. Ibrahim, M. Abdel-Rahman, Emad A. Badawi, M. A. Abdel-Rahman, Exp. Theo. NANOTECHNOLOGY 2 (2018) 85
[2] Uhlmann E, Sammler F. Adv Mater Res 907 (2014) 63
[3] Silva FJG, Fernandes AJS, Costa FM, Teixeira V, Baptista APM, Pereira E. Wear 255 (2003) 846
[4] Yang N, Ed. Novel Aspects of Diamond: From Growth to Applications. Berlin: Springer; (2015)
[5] Szunerits S, Nebel CE, Hamers RJ. MRS Bulletin 39 (2014) 517
[6] Aharonovich I, Neu E. Diamond nanophotonics. Adv Opt Mater 2 (2014) 911
[7] Prawer S, Aharonovich I. Quantum information processing with diamond: principles and applications. Elsevier; (2014)
[8] Neu E, Arend C, Gross E, *et al.* Appl Phys Lett 98 (2011) 243107
[9] Hui YY, Cheng C-L, Chang H-C. J Phys D: Appl Phys 43 (2010) 374021
[10] Wang L, Lei X, Shen B, Sun F, Zhang Z. Diam Relat Mater 33 (2013) 54
[11] Musale DV, Sainkar SR, Kshirsagar ST. Raman, Diam Relat Mater 11 (2002) 75
[12] Grudinkin SA, Feoktistov NA, Medvedev AV, *et al.* J Phys D: Appl Phys 45 (2012) 062001
[13] Cui Y, Zhang J, Sun F, Zhang Z. Trans Nonferrous Met Soc China 23 (2013) 2962
[14] Sedov VS, Ralchenko VG, Vlasov II, *et al.* Bull Lebedev Phys Inst 41 (2015) 359
[15] Smolin AA, Ralchenko VG, Pimenov SM, Kononenko TV, Loubnin EN. Appl Phys Lett 62 (1993) 3449

[16] Vlasov II, Goovaerts E, Ralchenko VG, Konov VI, Khomich AV, Kanzyuba MV. Diam Relat Mater 16 (2007) 2074
[17] Yim WM, Paff RJ. J Appl Phys 45 (1974) 1456
[18] Ager JW. Residual Stress in Diamond and Amorphous Carbon Films. Symposium I - Mechanical Behavior of Diamond and Other Forms of Carbon. 1995.
[19] Bolshakov A, Ralchenko V, Sedov V, et al. Phys Status Solidi A 488 (2015) 57
[20] Sternschulte H, Thonke K, Sauer R, Münzinger PC, Michler P. Phys Rev B 50 (1994) 14554
[21] Sedov V, Ralchenko V, Khomich AA, Diam Relat Mater. 56 (2015) 23
[22] Burns RC, Cvetkovic V, Dodge CN, J Cryst Growth. 104 (1990) 257
[23] Rogers LJ, Jahnke KD, Doherty MW, Phys Rev B. 89 (2014) 235101
[24] Turukhin AV, Liu C-H, Gorokhovsky AA, Alfano RR, Phillips W. Phys Rev B. 54 (1996) 16448
[25] Davydov VA, Rakhmanina AV, Lyapin SG, Jetp Lett. 99 (2014) 585
[26] Fabisiak K, Ba{a W, Paprocki K, Szreiber M, Uniszkiewicz C. Opt Mater. 31 (2009) 1873
[27] Smith BR, Gruber D, Plakhotnik T. Diam Relat Mater. 19 (2010) 314
[28] Singh S, Thomas V, Martyshkin D, Kozlovskaya V, Kharlampieva E, Catledge SA. Nanotechnology 25 (2014) 045302
[29] Sovyk D, Ralchenko V, Komlenok M, Appl Phys A. 118 (2014) 17

Exp. Theo. NANOTECHNOLOGY 3 (2019) 247-261